ACS OMEGA

Open Access

http://pubs.acs.org/journal/acsodf

Article

Hydrolysis Kinetics of Low-Concentration Industrial $TiOSO_4$ Solution and Structural Evolution of Metatitanic Acid

Congxue Tian* and Hua Chen

Cite This: *ACS Omega* 2023, 8, 34826−34833

Read Online

ACCESS | Metrics & More | Article Recommendations

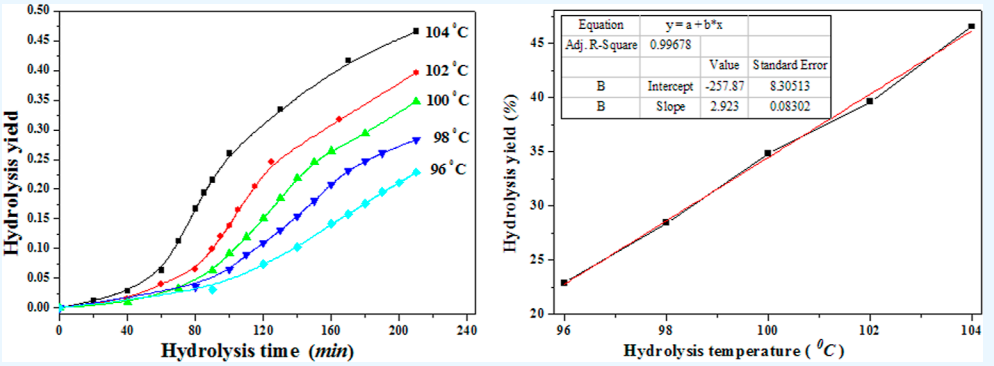

ABSTRACT: Using the industrial low-concentration $TiOSO_4$ solution as the raw material, the hydrolysis kinetics and structural evolution of metatitanic acid was investigated. The samples were characterized by TiO_2 content, XRD analysis, particle size distribution, FT-IR spectroscopy, Raman analysis, and HRTEM. The curves of hydrolysis yield showed *S* type shape, and the hydrolysis process consisted of the induction period, rapid hydrolysis period, and mature period. The rapid hydrolysis period was the first-order reaction, and increasing of hydrolysis temperature would shorten the induction period and hydrolysis period while prolonging the mature period had an approximate linear positive correlation on the hydrolysis yield and hydrolysis rate. The actual hydrolysis yield at the graying point was consistent with the calculated hydrolysis yield. The calculated pre-exponential factor k_0 was 1.40×10^{18} min^{-1} and activation energy E_a was of 147.6 kJ/mol. With the hydrolysis temperature increasing, the grain size increased, the lattice stress decreased, the average particle size of metatitanic acid decreased, and the sulfur content decreased, resulting from the growth and adjustment of crystals and colloidal particles. Also, the SO_4^{2-} ions promoted the formation of anatase TiO_2 crystals. The formation of the precipitated particles underwent processes such as gel, crystal growth, aggregation, and condensation.

1. INTRODUCTION

As the third largest inorganic chemical, titanium dioxide is widely used in many fields due to its excellent performance, and its market demand is enormous. The industrial production methods of TiO_2 are the sulfate process and the chloride process. Hydrolysis of industrial $TiOSO_4$ solution is the core step in the preparation of TiO_2 by the sulfate process, which is a complex physiochemical process, having a prominent impact on the particle size and its distribution of metatitanic acid (hydrated TiO_2, abbreviated as MA) and ultimately determines the structure, quality, and applications of the final TiO_2 pigment. The hydrolysis product of the $TiOSO_4$ solution is orthotitanic acid ($Ti(OH)_4$) at a lower temperature (25−80 °C) while the product became MA ($TiO(OH)_2$) at a higher temperature (80−110 °C).[1] The formation of MA in the thermal hydrolysis of $TiOSO_4$ solution goes through a series of steps, involving an ionic reaction, olation and oxolation, nucleation, grain growth, and aggregating to the final precipitation form.[2] Reaction kinetics is the study of the effects of various physical and chemical factors (such as temperature, pressure, concentration, medium in the reaction system, catalyst, flow field, temperature distribution, etc.) on the reaction rate, as well as the corresponding reaction mechanism and mathematical expressions. The concentration of titanyl sulfate and sulfuric acid obviously influenced the kinetics of the titania film growth, following the sigma type.[3] By investigating the influence and hydrolysis kinetics in $TiOSO_4$ solution by the sodium hydroxide molten salt method, it was found that the main influence factors in the hydrolysis process were the initial concentrations of $TiOSO_4$ and sulfuric

Received: June 8, 2023
Accepted: August 31, 2023
Published: September 14, 2023

acid.[4] The transition from the amorphous state to crystalline anatase phase was determined according to the Kissinger's equation, and the calculated activation energy (E_a) was of 160 ± 2 kJ/mol and the rate constant (k_0) was of 2.86 × 10^{11} min^{-1}.[5] The influences of hydrolysis factors and the characteristics of precipitation of $TiOSO_4$ solution were also investigated, and the obtained population balance equations could be used to calculate the average size of the elementary particles and the aggregates during the hydrolysis process.[2] The precipitation kinetics, nucleation, and growth mechanism at a temperature range of 70−90 °C and a Ti^{4+} concentration of 0.5−1.5 mol/L were investigated, by using forced hydrolysis of aqueous $TiCl_4$ solution to produce rutile nanostructured powders. It was found that the precipitation kinetics followed the *Avrami* model, exhibiting a slow induction nucleation stage and an accelerating growth stage.[6] The hydrolysis degree of $TiOSO_4$ conversion to the hydrated TiO_2 clearly depended on the concentrations of Fe^{2+} and Fe^{3+}, the Fe^{2+} (up to 5 wt %) had significant promoting effects on the hydrolysis process and the hydrolysis conversion degree while Fe^{3+} exhibited inhibitory effects on the hydrolysis process.[7] There were two mainstream theories of the hydrolysis mechanism of Ti^{4+} ions, which could be described as H^+ ion transfer theory and colloid aggregation theory. The TiO_2 morphology was highly dependent on concentrations of $TiOSO_4$, and the $TiOSO_4$ concentration exerted a strong influence on the shape and surface structure of the produced TiO_2 particles. The resultant TiO_2 consisted of round agglomerates of 5−10 nm primary particles at a higher concentration of $TiOSO_4$, and the size of secondary particles depended mainly on the H_2SO_4 concentration.[8] The hydrolysis of Ti^{4+} ions relied on a bonding rearrangement process inside an inorganic polymer causing crystalline phase formation,[9] and the hydrolysis degree and particle size of the obtained hydrated titanium dioxide depended on the initial concentration of $TiOSO_4$ and H_2SO_4.[10] The electrokinetic measurements of the anatase TiO_2 formed by the sol−gel method suggested that the dopant ions tended to accumulate on the surface of the particles.[11] The hydrolysis conditions of the $TiOSO_4$ solution affected the structures, compositions, and properties of hydrated MA and TiO_2.[12−16] The hydrolysis system of the industrial $TiOSO_4$ solution was very complex due to its high concentration of $TiOSO_4$, H_2SO_4, ferrous ion, and other impurities, which could increase the density, viscosity, and total ion concentration of the solution and affect the hydrolysis process and the precipitation of MA. Most literature on the hydrolysis of Ti^{4+} used pure titanium sources such as tetrabutyl titanate, $TiCl_4$, or $Ti(SO_4)_2$ as hydrolysis raw materials.[17−19] Compared to the actual use of high-concentration industrial $TiOSO_4$ solution in traditional TiO_2 production, low-concentration industrial $TiOSO_4$ solution can save energy consumption caused by the concentration, playing a very important role in energy conservation and consumption reduction. Unlike previous literature reports, the hydrolysis kinetics of low-concentration $TiOSO_4$ solution was conducted under the conditions of high TiO_2 concentration, high acidity, and high impurity content, which would have different effects on the hydrolysis rate, nucleation process, crystal and particle growth, aggregation process, etc. Also, these effects would ultimately determine the structure and application performances of MA and TiO_2. Studying the hydrolysis kinetics of a low-concentration industrial $TiOSO_4$ solution was of great value for practical TiO_2 production control and the quality of MA while there were few reports on the hydrolysis kinetics of industrial $TiOSO_4$ systems.

The aim of this work was to investigate the hydrolysis kinetics of low-concentration industrial $TiOSO_4$ solution and its effects on the hydrolysis yield and structure of MA, which would be of great significance to control the hydrolysis conditions to obtain hydrolyzed MA with a good structure and high yield.

2. EXPERIMENTAL SECTION

2.1. Hydrolysis Kinetics Experiments. The hydrolysis kinetics experiments of the low-concentration industrial $TiOSO_4$ solution were conducted in a flask with stirring and condensation reflux and placed in an oil bath in a thermostat. The industrial $TiOSO_4$ solution was taken from a titanium dioxide factory in Panzhihua, with a total TiO_2 concentration of 184 g/L, F value of 1.91 (F value meant the mass ratio of free sulfuric acid and sulfuric acid combined with Ti^{4+} to TiO_2, with a free H_2SO_4 concentration of 1.29 mol/L), Fe/TiO_2 of 0.39 (with Fe^{2+} ion content of 1.28 mol/L), and Ti^{3+} ion of 2.14 g/L. The typical hydrolysis reactions were carried out at the temperature of 96, 98, 100, 102, and 104 °C via the authigenic seed thermal hydrolysis method as the following steps and controlling the temperature fluctuations within a range of ±0.1 °C. Deionized water with a 15% volume ratio (60 mL) as to the $TiOSO_4$ solution was used as the induced water and was preheated to 96 °C in the flask. The industrial $TiOSO_4$ solutions with the corresponding one volume (400 mL) placed in the beaker were separately preheated to the hydrolysis temperature as mentioned above, then pumped into the induced water through the peristaltic pump in 20 min, and then, the setting hydrolysis temperature was maintained. After the hydrolysis mixture turned to gray color, the slurry was extracted from the hydrolysis system at different times as the analytical samples. The extracted slurry was immediately cooled with ice water and separated at the speed of 12,000 rpm for 10 min with a high-speed centrifuge. Supernatant obtained by centrifugation was used to determine its TiO_2 concentration for calculating the hydrolysis yield. Using the end of feeding as the beginning of hydrolysis time (t = 0 min), the hydrolysis process was completed after 210 min at different hydrolysis temperatures. The slurry was filtered and washed with 2000 mL of deionized water, and a portion of the MA filter cake was dried at 105 °C for 2 h and then the MA samples were obtained, marked as 1#, 2#, 3#, 4#, and 5#, respectively.

2.2. Characterization. The hydrolysis yield was determined by measuring TiO_2 content in the supernatant, according to the standard ISO 591-1:2000 "*Titanium dioxide pigments for paints*", hydrolysis yield (η) was calculated using $\eta = (C_0 - C_t)/C_0$, where C_0 is the initial Ti^{4+} concentration and C_t is the Ti^{4+} concentration hydrolyzed at t min. The crystal structure of the MA samples was determined by an X-ray diffractometer (X' Pert3Powder, PANalytical), and the anatase grain size $L_{(101)}$ for crystal plane (101) was calculated according to the Scherrer equation. The lattice strain of MA crystals in the C-axis direction was obtained by refining the crystal structure through the *reflex module* of Materials Studio software. Particle size distribution of the MA samples was determined with a Malvern particle size analyzer (Mastersizer 2000, Malvern). The FT-IR test and analysis were carried out on an infrared spectrometer (Nicolet-380, Thermo, USA). Raman spectra for the MA samples were obtained from a

https://doi.org/10.1021/acsomega.3c04035
ACS Omega 2023, 8, 34826−34833

micro confocal Raman spectroscopy by using a laser with a wavelength of 532 nm for measurement (inVia, Renishaw, UK). The morphology and the lattice fringes of sample 5# were determined by a field-emission transmission electron microscope (Tecnai G2 F20 S-TWIN, USA). The sulfur content of MA was measured on a high-frequency infrared carbon sulfur analyzer (CS230, Leco, Thermo Fisher).

3. RESULTS AND DISCUSSION

The curves of hydrolysis yield for industrial $TiOSO_4$ solution at different times are shown in Figure 1. It showed that the

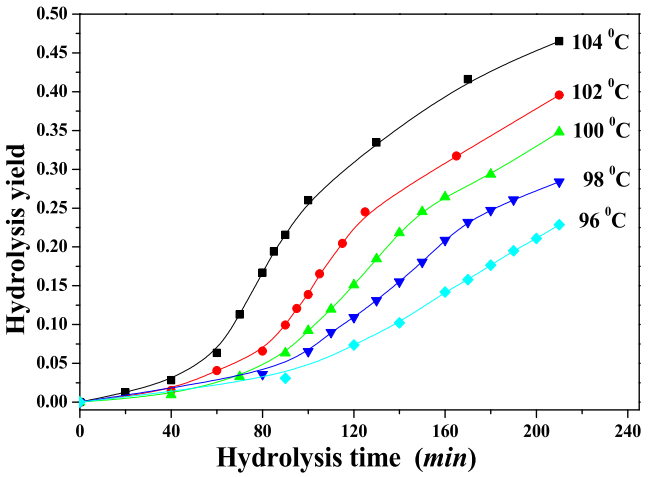

Figure 1. Curves of hydrolysis yield at different hydrolysis times.

hydrolysis yield increased gradually with the hydrolysis time increasing, and the curves were in shapes of *S* type. The lower hydrolysis the temperature was, the smaller the hydrolysis yield was, and the hydrolysis yield gradually increased with the increase of hydrolysis temperature. The hydrolysis yield curves could be divided into three sections, the induction period, rapid hydrolysis period, and mature period. In the induction period, due to a small amount of hydrolyzed seed in the solution, the hydrolysis yield was very small and changed slowly, and the activity of nucleus seed was high. At this stage, the hydrolysis system mainly formed crystal nuclei to induce the hydrolysis process. After forming a large number of hydrolysis nucleus at the end of the induction period, the hydrolysis reaction turned into the rapid hydrolysis period and the hydrolysis yield changing curve showed a steep straight line upward. This indicated that the hydrolysis reaction at this stage was mainly a first-order reaction controlled by the surface growth of hydrated TiO_2 particles. After that, the hydrolysis reaction turned into the mature period; it was mainly controlled by the surface diffusion process as the free Ti^{4+} concentration used to form crystals decreased, the positive driving force of the hydrolysis reaction gradually weakened, leading to a gradual decrease in the hydrolysis rate. With hydrolysis temperature increasing, the induction period and the hydrolysis period were shortened, while the mature period was prolonged, and the hydrolysis rate was accelerated obviously.

The derivative curves of hydrolysis yield at different hydrolysis times are shown in Figure 2. The changes of the hydrolysis rate could clearly be seen, indicating the velocity of the hydrolysis reaction rate. The maximum values of the curves corresponded to the graying point, with the fastest hydrolysis

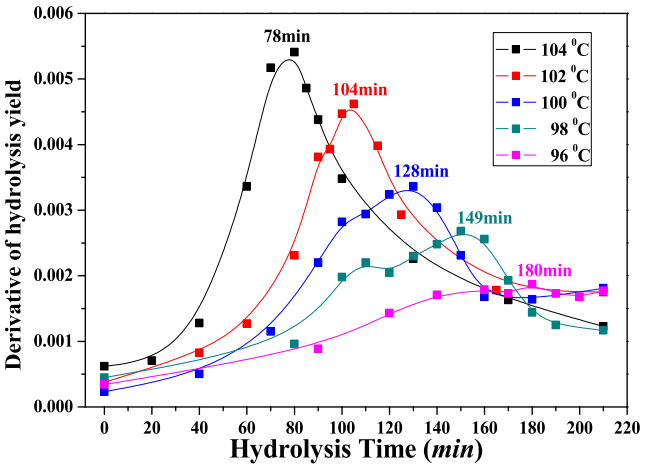

Figure 2. Derivative curves of hydrolysis yield at different hydrolysis times.

rate. The steepness of the curve changes also reflected the hydrolysis velocity, with the steeper the curve, the faster the hydrolysis rate. In the induction period, the hydrolysis rate was very slow. After turning into the hydrolysis period, the hydrolysis rate rapidly increased until reaching the maximum value at the graying point and then gradually decreased. As the hydrolysis proceeded, the total TiO^{2+} ion concentration decreased, and the hydrolysis rate gradually stabilized and turned into the mature stage. When $TiOSO_4$ solution was hydrolyzed, a large number of colloidal microcrystals (7−8 nm) were first formed, and then, these microcrystals aggregated and formed the primary agglomerates (60−100 nm). The size and distribution of these primary agglomerates were important factors to determine the structure, properties, and applications of TiO_2. The primary agglomerates reaggregated to form the secondary aggregates with a particle size of 1−2 μm, which was the final appearance of MA precipitation particles.[20,21]

In the rapid hydrolysis period, there was a linear relationship between the hydrolysis yield and hydrolysis time due to its first-order reaction. By linear regression, the corresponding regression equations at different hydrolysis temperatures were obtained using eqs 1−5. The regression correlation coefficient R^2 values were all greater than 0.99, indicating that the linear correlation of the regression fitting equation was very significant. The coefficient of hydrolysis time in the regression equation reflected the magnitude of the hydrolysis rate, indicating that hydrolysis temperature played a very important role in the hydrolysis reaction rate. The higher the hydrolysis temperature, the faster the hydrolysis rate. The reaction rate would increase by 0.358 times for every 1 °C increase of the hydrolysis temperature.

$$104\ ^\circ\mathrm{C}: \eta = 0.00498t - 0.23379 \qquad R^2 = 0.9981 \tag{1}$$

$$102\ ^\circ\mathrm{C}: \eta = 0.00406t - 0.26321 \qquad R^2 = 0.9978 \tag{2}$$

$$100\ ^\circ\mathrm{C}: \eta = 0.00308t - 0.21667 \qquad R^2 = 0.9989 \tag{3}$$

$$98\ ^\circ\mathrm{C}: \eta = 0.00249t - 0.19159 \qquad R^2 = 0.9987 \tag{4}$$

https://doi.org/10.1021/acsomega.3c04035
ACS Omega 2023, 8, 34826−34833

$$96\ ^{\circ}\mathrm{C}: \eta = 0.00180t - 0.14782 \qquad R^2 = 0.9990 \tag{5}$$

where η is the hydrolysis yield and t is the hydrolysis time in minute unit.

The time and hydrolysis yield at the graying point at different hydrolysis temperatures are listed in Table 1. The

Table 1. Time and Hydrolysis Yield at the Graying Point at Different Hydrolysis Temperatures

no	hydrolysis temperature (°C)	actual graying point time (min)	calculated graying point time (min)	actual hydrolysis yield (%)	calculated hydrolysis yield (%)
1#	96	180	180	17.7	17.6
2#	98	152	149	17.9	17.9
3#	100	125	128	17.1	17.7
4#	102	105	104	16.5	15.9
5#	104	80	78	16.7	15.5

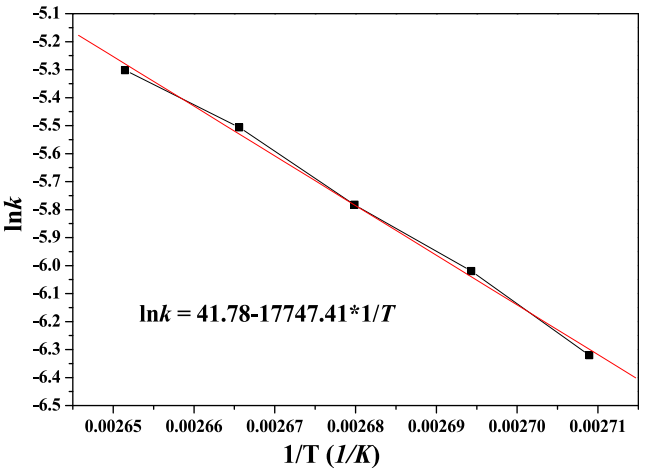

Figure 3. Curve of velocity constant at different hydrolysis temperatures.

higher the hydrolysis temperature, the shorter the time for the hydrolysis system to reach the graying point. In a certain concentration of the $TiOSO_4$ solution hydrolysis system, there was a good linear relationship between the graying point time and the hydrolysis temperature, which was negatively correlated. At different hydrolysis temperatures, the actual graying point time and calculated graying point time were basically the same, with a relative error of within 2.5%, indicating that the fitting equations were more accurate in evaluating the graying point. The actual hydrolysis yield at the graying point ranged from 16.5 to 17.9%, while the calculated hydrolysis yield ranged from 15.5 to 17.9%, with a relative error of less than 7.2%, meeting the requirements of industrial production for controlling the hydrolysis graying point. There were two main reasons for the higher actual hydrolysis yields compared to the calculated ones. On the one hand, the sampling and separation process would take a certain amount of time, leading to an increase in hydrolysis yield. On the other hand, due to the small size of MA particles, there was no significant color change when reaching the graying point, leading to a delay in the artificial determination of the graying point, and resulting in a high hydrolysis yield. The prediction of hydrolysis yield and judgment of the graying point were of great significance for the actual TiO_2 production control.

The relationship between the rate constant of a chemical reaction and temperature satisfied the Arrhenius equation $k = k_0 \times E_a/RT$. The following eq 6 was obtained by taking the natural logarithm on both sides of the equation.

$$\ln k = \ln\ k_0 - \frac{E_a}{R} \times \frac{1}{T} \tag{6}$$

Using $\ln k$ as the vertical axis and $1/T$ as the horizontal axis, we fitted the equations at different hydrolysis temperatures and obtained a linear relationship between $\ln k$ and $1/T$, as shown in Figure 3.

Also, obtained the linear regression as expressed in eq 7

$$\ln k = 41.78 - 17747.41 \times \frac{1}{T} \mathrm{R}^2 = 0.997 \tag{7}$$

The pre-exponential factor k_0 of the hydrolysis reaction calculated by substituting the fitted values obtained was 1.40×10^{18} min^{-1}, and the activation energy E_a was of 147.6 kJ/mol. The value of E_a showed great influences of temperature on the hydrolysis rate for the $TiOSO_4$ solution. The calculated activation energy E_a was higher than that reported in the literature.[22] This might be due to the fact that when the hydrolysis reaction was carried out under a high concentration and acidity, high acidity inhibited the hydrolysis reaction, which increased the activation energy of the hydrolysis reaction. Also, the corresponding ionic strength of a high-concentration $TiOSO_4$ solution was larger, the effective concentration actually involved in the reaction was lower, which weakened the effective collision, and the energy barrier through which the reaction passed was higher, resulting in a higher apparent activation energy.

The hydrolysis yield, compositions, and structures for MA at different hydrolysis temperatures are listed in Table 2. As the hydrolysis temperature increased, the hydrolysis rate increased, and the hydrolysis yield of the $TiOSO_4$ solution gradually increased, showing a linear positive correlation as shown in Figure 4, with a linear correlation coefficient R^2 of 0.99678. This was closely related to the temperature-promoting effects on the hydrolysis reaction rate.

The XRD patterns for the MA samples obtained at different hydrolysis temperatures are shown in Figure 5, agreeing obviously with the standard anatase TiO_2 phase (JCPDS 21-1272), proving their anatase crystal. With the hydrolysis temperature increasing, the peak intensity increased, and the peak width narrowed, showing that the crystallinity of the MA crystals gradually increased. As the hydrolysis temperature increased from 96 to 102 °C, the grain size $L_{(101)}$ ranged from 8.7 to 10.1 nm in Table 2, presenting an approximate linear relationship, indicating that the growth of MA crystals below the boiling point was controlled by the diffusion of constructing crystal ions and surface growth. Under the boiling hydrolysis state, the grain size of MA crystals rapidly grew to 11.8 nm, mainly due to the increase in the hydrolysis temperature and the enhancement of system disturbance stirring. The Ti^{4+} ions had higher polarizability, which could bind hydroxyl groups to form the complexes such as $[Ti(OH)_2SO_4(H_2O)_3]^0$ and $[Ti(OH)_2(SO_4)_2(H_2O)_2]^{2-}$. In the $TiOSO_4$ solution, the complexes could constitute the $Ti-O_6$ octahedron.[23,24] The presence of SO_4^{2-} ions would alter the hydrolysis process of $TiOSO_4$ solution, resulting in a lower hydrolysis nucleation temperature, longer nucleation time, and wider temperature range.[25] Because the hydroxyl sites were

https://doi.org/10.1021/acsomega.3c04035
ACS Omega 2023, 8, 34826−34833

Table 2. Hydrolysis Yield, Compositions, and Structures for MA at Different Hydrolysis Temperatures

no	temperature (°C)	hydrolysis yield (%)	$L_{(101),MA}$ (nm)	lattice strain (%)	$D_{50,\ MA}$ (μm)	$D_{AV,\ MA}$ (μm)	S (%)
1#	96	22.87	8.7	0.548	1.42	1.52	12.15
2#	98	28.41	9.1	0.539	1.38	1.47	8.76
3#	100	34.78	9.5	0.537	1.34	1.43	7.64
4#	102	39.57	10.1	0.531	1.28	1.37	5.23
5#	104	46.52	11.8	0.524	1.22	1.33	3.56

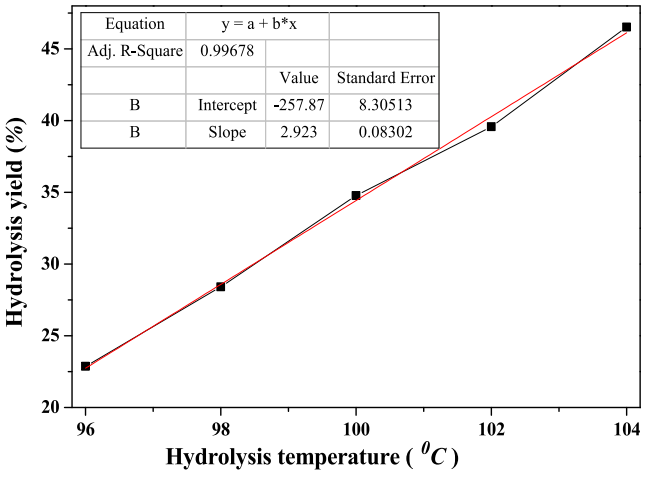

Figure 4. Hydrolysis yield regression curve at different hydrolysis temperatures.

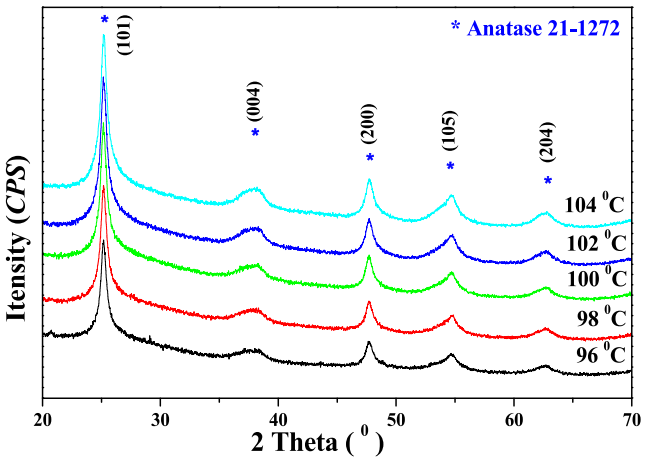

Figure 5. XRD patterns of MA obtained at different hydrolysis temperatures.

occupied by SO_4^{2-} ions, the SO_4^{2-}ions were bound to the Ti−O bond through chelating coordination and bidentate coordination, and the corresponding anatase phase was formed by edge arrangement of the Ti−O_6 octahedron. At the same time, the TiO^{2+} ions were easily connected to each other to form multiple nuclei, due to its large specific surface area, colloidal structure, and strong surface tension, and they were more prone to aggregation. Moreover, the aggregation rate of the primary crystals and colloidal particles was much greater than the crystallization rate, which caused most of the precipitated particles to form an amorphous TiO_2 structure. Only a small amount of anatase TiO_2 arranged with the corresponding crystal structure, which could be reflected by the XRD diffraction peak width. The lattice strain for the MA crystals showed a slightly decreasing trend, decreasing from 0.548 to 0.524%. When the hydrolysis temperature was low, the corresponding grain size was small, the structure was relatively loose, and the corresponding lattice stress was high. After the hydrolysis temperature increased, the grain growth accelerated, the crystal structure became more compact, the lattice arrangement became more regular, and the corresponding lattice stress gradually decreased. The minimum lattice strain was 0.524% at the boiling point, indicating that the boiling point temperature helped to reduce lattice stress, promote grain growth, and obtain well-structured MA crystals.

The $D_{50,\ MA}$ and $D_{AV,\ MA}$ for the wet MA samples are also listed in Table 2. With the hydrolysis temperature increasing, the average particle size ($D_{AV,\ MA}$) decreased from 1.52 to 1.33 μm, and the $D_{50,\ MA}$ decreased from 1.42 to 1.22 μm. The measured particle size corresponded to the secondary aggregates, which were formed by the primary agglomerates composed of many crystal particles. Due to the presence of a large number of crystals in the system, with the crystal size of MA crystals increasing, the primary agglomerates would be larger, and the secondary aggregates would be smaller. The sulfur content (S %) in Table 2 showed a gradually decreasing trend with the increase of hydrolysis temperature, ranging from 12.15 to 3.56%. This was mainly due to the small crystal size, strong colloidal properties, and more sulfate ions, whose role was to reunite the primary agglomerates into the secondary aggregates, closely related to the structure and colloidal properties of MA obtained at different temperatures.

About 95% of water and 16% of H_2SO_4 would be removed from MA after drying at 105 °C.[26] The FT-IR spectra for the MA samples are shown in Figure 6. The FT-IR peaks at about 1628 cm^{-1} were the bending vibration peaks of the physically adsorbed molecular water H−O−H, and the absorption shoulder peaks with a wide range of 3400−3500 cm^{-1} were the stretching vibration of surface hydroxyl O−H.[27] The peaks at 1039 and 1137 cm^{-1} were the characteristic absorption

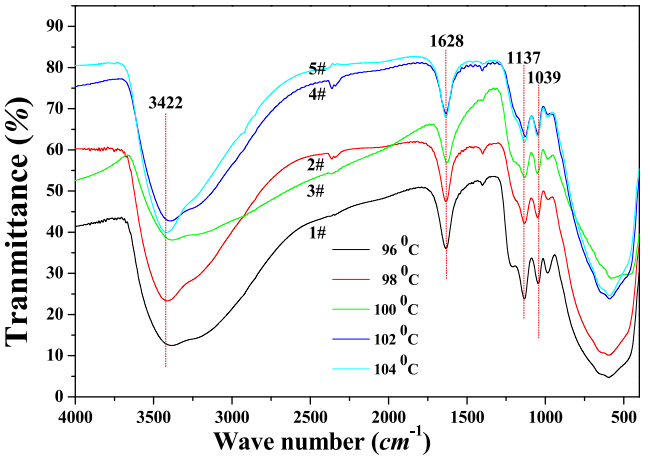

Figure 6. FT-IR spectra for MA obtained at 104 °C.

https://doi.org/10.1021/acsomega.3c04035
ACS Omega 2023, 8, 34826−34833

peaks of the bidentate coordination sulfate ion,[28,29] which bonded with Ti−O and possessed the properties of super acids.[30] The presence of sulfate ions and water would help the MA particles to form pore structures during the hydrolysis process.[31] There was a positive correlation between the relative intensity of the sulfate peaks and the sulfur content in MA. As the hydrolysis temperature increased, the infrared absorption intensity of sulfate ions gradually weakened, indicating a decrease in sulfur content in the MA samples, which was consistent with the measurement results of the *S* content in Table 2.

The Raman spectra for the MA samples are shown in Figure 7. The spectral deconvolution was used to determine the peak

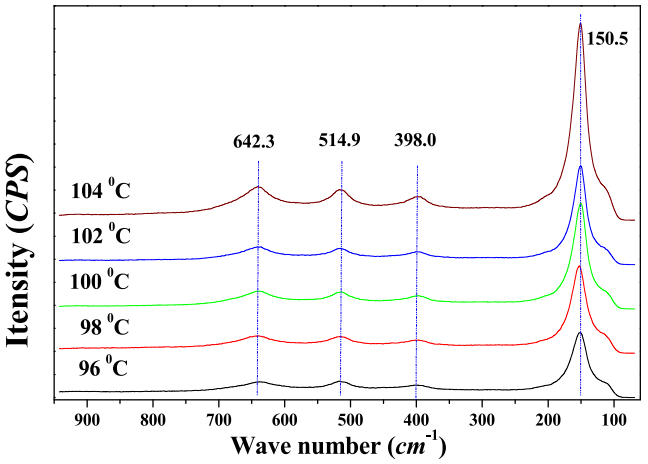

Figure 7. Raman spectrum for MA obtained at 104 °C.

position and width, and the peak positions were consistent with the Raman shift of anatase TiO_2. The phonon confinement model was used to explain the broadening and shifts of the Raman line shapes.[32,33] As hydrolysis temperature increased, the peak positions shifted to the higher wavenumber position, and its corresponding peak width also narrowed, indicating that the grain size of the MA samples increased, which was consistent with the previous XRD analysis.

The HRTEM photograph for sample 5# is shown in Figure 8. The photograph showed there were only discontinuous anatase-phase lattice fringes in the MA crystals, and the fringe spacing was 0.352 nm, corresponding to the anatase (101)

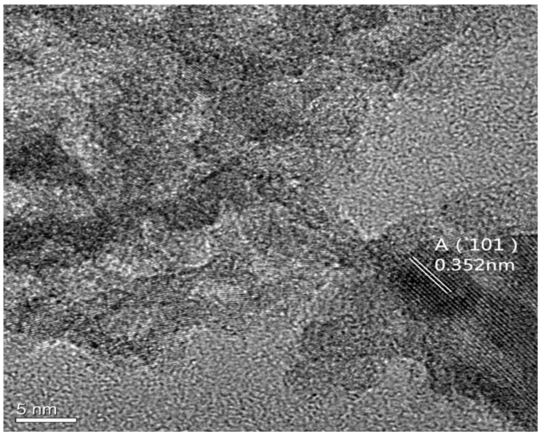

Figure 8. HRTEM photograph for sample 5.

crystal plane spacing. However, most images did not show lattice fringes, indicating that MA particles mainly existed in an amorphous form, which was consistent with the results of XRD diffraction with wide peaks and a small grain size. Supersaturation, the driving force for crystallization was examined from a thermodynamic perspective and combined with the Burton−Cabrera−Frank crystal growth model to obtain a simple and consistent method to analyze crystal growth data and obtain kinetics with only a single constant.[34] The smaller particles, aggregated on the surface of nucleus seed particles, would continue to grow in size during precipitation.[21] The larger anatase particles formed by directional aggregation between smaller anatase particles. The large binding energy of the Ti−O bond tended to align and sterically hinder SO_4^{2-} bonded on the surface of the small grains, resulting in a fan-shaped arrangement of lattice fringes.

The hydrolysis of the $TiOSO_4$ solution was begun with the gel form. The hydrated TiO_2 gel with an electric double layer was formed by olation and oxolation of Ti−O−Ti in the induction period in the $TiOSO_4$ hydrolysis system. The center of the electric double layer was hydrated anatase TiO_2 acting as induced nuclei, the inner layer included SO_4^{2-} and H_2O, and the outer layer included H^+ and H_2O. The charges of the electric double layer depended on the pH and SO_4^{2-} concentration. The electric double layer between small particles and the presence of SO_4^{2-} would prevent nucleation, crystal growth, and aggregation. The TiO_2 colloidal particles were induced with anatase-phase structure as nuclei, and the nuclei activity depended on the number of suspended unsaturated bonds on its surface and the hydrolysis conditions (temperature and pH). The smaller anatase nucleus particles were formed directly from the $TiOSO_4$ solution, through the combined effects of homogeneous and secondary nucleation.[21] When the number of nuclei reached a certain number, the hydrolysis rate increased rapidly, and the hydrolysis process turned into a rapid hydrolysis period, where the agglomeration and aggregation of the hydrated TiO_2 particles began to dominate.

4. CONCLUSIONS

The hydrolysis kinetics of industrial low-concentration $TiOSO_4$ solution and structure changes of MA have been investigated in detail. The curves of hydrolysis yield at different times were in shapes of *S* type, and the hydrolysis process could be divided into the induction period, rapid hydrolysis period, and mature period. In the rapid hydrolysis period, hydrolysis was a first-order reaction, controlled by the surface growth of hydrated TiO_2 particles. When the hydrolysis reaction reached the graying point, the actual hydrolysis yield at the graying point ranged from 16.5 to 17.9% at different temperatures, basically consistent with the calculated hydrolysis yield. The hydrolysis temperature had an approximate linear positive correlation on the hydrolysis yield and hydrolysis rate. According to the hydrolysis kinetics calculations, the pre-exponential factor k_0 was 1.40×10^{18} min^{-1}, and the activation energy E_a was of 147.6 kJ/mol. With the hydrolysis temperature increasing, the grain size gradually increased, the lattice stress decreased, promoting the growth and adjustment of crystals and colloidal particles for MA, and the corresponding average particle size of MA gradually decreased. The higher the hydrolysis temperature, the lower the sulfur content, which was determined by the structure and colloidal properties of MA. The presence of SO_4^{2-} ions

https://doi.org/10.1021/acsomega.3c04035
ACS Omega 2023, 8, 34826−34833

promoted the formation of anatase TiO_2 crystals, and the obtained MA particles were predominantly amorphous components, containing a small amount of anatase crystal structure, formed by the induction and the steric hindrance of SO_4^{2-} ions in the bidentate ligand on the MA surface. The gel structure of MA was first formed in the $TiOSO_4$ hydrolysis system and then the corresponding precipitated particles of MA were gradually formed through crystal growth, aggregation, condensation.

■ ASSOCIATED CONTENT

Data Availability Statement

All data generated or analyzed during this study are included in this manuscript.

■ AUTHOR INFORMATION

Corresponding Author

Congxue Tian − *Panzhihua University, Panzhihua 617000 Sichuan, P. R. China;* orcid.org/0000-0001-8482-0169; Email: tcx7311@163.com

Author

Hua Chen − *Panzhihua University, Panzhihua 617000 Sichuan, P. R. China*

Complete contact information is available at: https://pubs.acs.org/10.1021/acsomega.3c04035

Author Contributions

The author *Congxue Tian* obtained all the funding, proposed the relevant concepts and methods, designed experiments, conducted experimental research, and wrote and revised the manuscript. The author *Hua Chen* carried out the experiments and measurements and wrote and revised the manuscript.

Notes

The authors declare no competing financial interest.

■ ACKNOWLEDGMENTS

This study was supported by the Natural Science Foundation of Sichuan Province (2022NSFSC0307), Major Scientific and Technological Research Project of Panzhihua Xichang Strategic Resource Development (CCJ [2022] no. 390-1-9), Science and Technology Achievement Transfer and Transformation Guidance Plan of Sichuan Province (23ZHSF0237), Sichuan Provincial Science and Technology Plan Transfer Payment Special Project (22ZYZF-GG-02, 22ZYZF-GG-05), and Science and Technology Service Industry Project of Sichuan Province (2022GFW001-04, Xingzhong Titanium Industry).

■ REFERENCES

(1) Middlemas, S.; Fang, Z. Z.; Fan, P. A new method for production of titanium dioxide pigment. *Hydrometallurgy* **2013**, *131*−*132*, 107−113.

(2) Santacesaria, E.; Tonello, M.; Storti, G.; Pace, R.; Carrà, S.; Carra, S. Kinetics of titanium dioxide precipitation by thermal hydrolysis. *J. Colloid Interface Sci.* **1986**, *111*, 44−53.

(3) Bavykin, D. V.; Savinov, E. N.; Smirniotis, P. G. Kinetics of the TiO_2 films growth at the hydrothermal hydrolysis of $TiOSO_4$. *React. Kinet. Catal. Lett.* **2003**, *79*, 77−84.

(4) Wang, W. J.; Chen, D. S.; Chu, J.; Li, J.; Xue, T. Y.; Wang, L. N.; Wang, D.; Qi, T. Influence and hydrolysis kinetics in titanyl sulfate solution from the sodium hydroxide molten salt method. *J. Cryst. Growth* **2013**, *381*, 153−159.

(5) Stojanovic, B. D.; Marinkovic, Z. V.; Brankovic, G. O.; Fidancevska, E. Evaluation of kinetic data for crystallization of TiO_2 prepared by hydrolysis method. *J. Therm. Anal. Calorim.* **2000**, *60*, 595−604.

(6) Charbonneau, C.; Gauvin, R.; Demopoulos, G. P. Nucleation and growth of self-assembled nanofibre-structured rutile (TiO_2) particles via controlled forced hydrolysis of titanium tetrachloride solution. *J. Cryst. Growth* **2009**, *312*, 86−94.

(7) Grzmil, B.; Grela, D.; Kic, B.; Podsiadly, M. The influence of admixtures on the course of hydrolysis of titanyl sulfate. *Polym. J. Chem. Technol.* **2008**, *10*, 4−12.

(8) Bavykin, D. V.; Dubovitskaya, V. P.; Vorontsov, A. V.; Parmon, V. N. Effect of $TiOSO_4$ hydrothermal hydrolysis conditions on TiO_2 morphology and gas-phase oxidative activity. *Res. Chem. Intermed.* **2007**, *33*, 449−464.

(9) Tarasov, A.; Goertz, V.; Goodilin, E.; Nirschl, H. Hydrolytic stages of titania nanoparticles formation jointly studied by SAXS, DLS, and TEM. *J. Phys. Chem. C* **2013**, *117*, 12800−12805.

(10) Grzmil, B. U.; Grela, D.; Kic, B. Hydrolysis of titanium sulphate compounds. *Chem. Pap.* **2008**, *62*, 18−25.

(11) Tsevis, A.; Spanos, N.; Koutsoukos, P. G.; van der Linde, A. J.; Lyklema, J. Preparation and characterization of anatase powders. *J. Chem. Soc., Faraday Trans.* **1998**, *94*, 295−300.

(12) Tian, C. X. Internal influences of hydrolysis conditions on rutile TiO_2 pigment production via short sulfate process. *Mater. Res. Bull.* **2018**, *103*, 83−88.

(13) Sathyamoorthy, S.; Hounslow, M. J.; Moggridge, G. D. Influence of stirrer speed on the precipitation of anatase particles from titanyl sulphate solution. *J. Cryst. Growth* **2001**, *223*, 225−234.

(14) Szilágyi, I.; Königsberger, E.; May, P. M. Characterization of chemical speciation of titanyl sulfate solutions for production of titanium dioxide precipitates. *Inorg. Chem.* **2009**, *48*, 2200−2204.

(15) Grzmil, B.; Grela, D.; Kic, B. Effects of processing parameters on hydrolysis of $TiOSO_4$. *Polym. J. Chem. Technol.* **2009**, *11* (3), 15−21.

(16) Grzmil, B.; Grela, D.; Kic, B. Formation of hydrated titanium dioxide from seeded titanyl sulphate solution. *Chem. Pap.* **2009**, *63* (2), 217−225.

(17) Yan, P. Y.; Zhang, Y.; Zheng, S. L. Microscale spherical TiO_2 powder prepared by hydrolysis of $TiCl_4$ solution: Synthesis and kinetics. *Particuology* **2024**, *84*, 60−71.

(18) Kalaiarasi, S.; Jose, M. Kinetics of anatase phase transformation of TiO_2 NPs synthesized using controlled hydrolysis technique. *Appl. Phys. A: Mater. Sci. Process.* **2018**, *124* (9), 589.

(19) Mansour, S. A. Non-isothermal crystallization kinetics of nano-sized amorphous TiO_2 prepared by facile sonochemical hydrolysis route. *Ceram. Int.* **2019**, *45*, 2893−2898.

(20) Sathyamoorthy, S.; Moggridge, G. D.; Hounslow, M. J. Particle formation during anatase precipitation of seeded titanyl sulfate solution. *Cryst. Growth Des.* **2001**, *1*, 123−129.

(21) Sathyamoorthy, S.; Moggridge, G. D.; Hounslow, M. Controlling particle size during anatase precipitation. *AIChE J.* **2001**, *47*, 2012−2024.

(22) Duncan, J. F.; Richards, R. G. Hydrolysis of titanium (IV) sulphate solutions: 2. Solution equilibria, kinetics and mechanism. *N. Z. J. Sci.* **1976**, *19*, 179−183.

(23) Matijevic, E.; Budnik, M.; Meites, L. Preparation and mechanism of formation of titanium dioxide hydrosols of narrow size distribution. *J. Colloid Interface Sci.* **1977**, *61*, 302−311.

(24) Zhao, L. S.; Liu, Y. H.; Wang, L.; Zhao, H. X.; Chen, D. S.; Zhong, B. N.; Wang, J. C.; Qi, T. Production of rutile TiO_2 pigment from titanium slag obtained by hydrochloric acid leaching of vanadium-bearing titanomagnetite. *Ind. Eng. Chem. Res.* **2014**, *53*, 70−77.

(25) Zan, L.; Zhong, J. C.; Luo, Q. R. Influence factors on preparing process of TiO_2 nanoscale particles. *J. Inorg. Mater.* **1999**, *14*, 264−270.

(26) Ratajska, H.; Przepiera, A.; Wisniewski, M. Thermal transformations of hydrous titanium dioxide. *J. Therm. Anal. Calorim.* **1990**, *36*, 2131−2134.
(27) Sivakumar, S.; Krishna Pillai, P.; Mukundan, P.; Warrier, K. G. K. Sol-gel synthesis of nanosized anatase from titanyl sulfate. *Mater. Lett.* **2002**, *57*, 330−335.
(28) Yamaguchi, T.; Jin, T.; Ishida, T.; Tanabe, K. Structural identification of acid sites of sulfur-promoted solid super acid and construction of its structure on silica support. *Mater. Chem. Phys.* **1987**, *17*, 3−19.
(29) Li, X. B.; Nagaoka, K.; Lercher, J. A. Labile sulfates as key components in active sulfated zirconia for n-butane isomerization at low temperatures. *J. Catal.* **2004**, *227*, 130−137.
(30) Zhu, X. D.; Nanny, M. A.; Butler, E. C. Effect of inorganic anions on the titanium dioxide-based photocatalytic oxidation of aqueous ammonia and nitrite. *J. Photochem. Photobiol., A* **2007**, *185*, 289−294.
(31) Shen, J.; Luo, N.; Zhang, M. J.; Tian, C. X.; Zhang, Z. Synthesis and characterization of mesoporous TiO_2-SO_4^{2-}. *Chin. J. Catal.* **2007**, *28* (3), 264−268.
(32) Zhu, K. R.; Zhang, M. S.; Chen, Q.; Yin, Z. Size and phonon confinement effects on low-frequency Raman mode of anatase TiO_2 nanocrystal. *Phys. Lett. A* **2005**, *340*, 220−227.
(33) Mahdjoub, N.; Allen, N.; Kelly, P.; Vishnyakov, V. SEM and Raman study of thermally treated TiO_2 anatase nanopowders: Influence of calcination on photocatalytic activity. *J. Photochem. Photobiol., A* **2010**, *211*, 59−64.
(34) Mohan, R.; Myerson, A. S. Growth kinetics: a thermodynamic approach. *Chem. Eng. Sci.* **2002**, *57*, 4277−4285.

https://doi.org/10.1021/acsomega.3c04035
ACS Omega 2023, 8, 34826−34833